Optics Letters

Effective hyper-Raman scattering via inhibiting electromagnetically induced transparency in monolayer graphene under an external magnetic field

Shaopeng Liu,[1] Wen-Xing Yang,[1,2,*] Zhonghu Zhu,[1] Shasha Liu,[1] and Ray-Kuang Lee[2]

[1]Department of Physics, Southeast University, Nanjing 210096, China
[2]Institute of Photonics Technologies, National Tsing-Hua University, Hsinchu 300, Taiwan
*Corresponding author: wenxingyang@seu.edu.cn

Received 7 April 2016; revised 11 May 2016; accepted 18 May 2016; posted 18 May 2016 (Doc. ID 262608); published 15 June 2016

We propose and analyze an effective scheme to generate hyper-Raman scattering via inhibiting electromagnetically induced transparency (EIT) in a monolayer graphene under a magnetic field. By solving the Schrödinger–Maxwell formalism, we derive explicitly analytical expressions for linear susceptibility, nonlinear susceptibility, and generated Raman electric field under the steady-state condition. Based on dressed-state theory, our results show a competition between EIT and hyper-Raman scattering, and the hyper-Raman process is totally dominant when multiphoton destructive interference is completely suppressed. © 2016 Optical Society of America

OCIS codes: (270.1670) Coherent optical effects; (020.4180) Multiphoton processes; (190.5650) Raman effect.

http://dx.doi.org/10.1364/OL.41.002891

The study of nonlinear optics phenomena, including optical solitons [1,2], multiwave mixing process [3,4], high-order harmonic generation [5,6], and Raman scattering [7,8], has shown tremendous interest due to their potential applications in optical communications and quantum information processing [9–13]. Recent advances involving these nonlinear optical processes have resulted in the generation of competition mechanisms [14–17], such as competition between electromagnetically induced transparency (EIT) and Raman processes [14,15], and between multiphoton ionization processes and four-wave mixing [16]. In particular, it is of interest to explore the competition between the EIT and hyper-Raman processes that may be used for generation of short-wavelength coherent radiation, conversion of frequency, and nonlinear spectroscopy.

To date, the monolayer graphene under an external magnetic field appears to be a good candidate for providing an intriguing optical nonlinearity in the infrared (IR) region [18–20]. As a purely two-dimensional material, graphene has unique electronic and optical properties originating from the linear, massless dispersion of electrons near the Dirac point and the chiral character of electron states [21–23]. The magneto-optical properties of graphene and thin graphite layers can give rise to multiple absorption peaks and particular selection rules between Landau levels (LLs) [18,19,24]. Motivated by these properties, this graphene may be more valuable for manipulating a nonlinear competitive process. In this Letter, we present a theoretical investigation that enables us to study the competition between EIT and hyper-Raman scattering in monolayer graphene under an external magnetic field. Different from using destructive interference induced by a continuous-wave (cw) control field [25], our scheme is dependent upon multiphoton destructive interference involving the production and propagation of an internally generated Raman field. In addition, we reveal that the different competition situations depend on whether multiphoton destructive interference is quenched or well-developed, where hyper-Raman scattering can be totally dominant by inhibiting EIT.

The $2D$ graphene crystal structure with complete energy levels under an external magnetic field is shown in Fig. 1, where the original linear dispersion relation of graphene is replaced by the discrete LLs. Because of the special selection rules in present graphene, optical transitions within these appointed energy levels are dipole allowed via the relation $\Delta|n| = \pm 1$ (n is the energy quantum number). According to this selection rule, right-hand circularly (RHC) or left-hand circularly (LHC) polarized photons could be absorbed under the condition of $\Delta|n| = -1$ or $\Delta|n| = +1$ [18], respectively. The eigenenergies of discrete LLs are $\epsilon_n = \mathrm{sgn}(n)\hbar\omega_c\sqrt{|n|}$ with carrier frequency ω_c [19,20]. In comparison with LLs of the conventional $2D$ electron/hole system with a parabolic dispersion, LLs in graphene are unequally spaced, and their transition energies are proportional to $\sqrt{B}$ [19,20,26]. In general, a linearly polarized laser field can be decomposed into two circularly polarized elements, i.e., $\vec{E}_j = (\vec{e}_- E_j^- + \vec{e}_+ E_j^+)\exp(-i\omega_j t + i\vec{k}_j\cdot\vec{r}) +$ c.c. ($j = p, 2, 3, 4$), and $\vec{e}_-$ ($\vec{e}_+$) corresponds to the unit vector of the LHC (RHC)-polarized basis, which can be denoted as $\vec{e}_- = [\hat{x} - i\hat{y}]/\sqrt{2}$ ($\vec{e}_+ = [\hat{x} + i\hat{y}]/\sqrt{2}$). In detail, the optical field of RHC-polarized component E_p^+ (E_2^+) with carrier

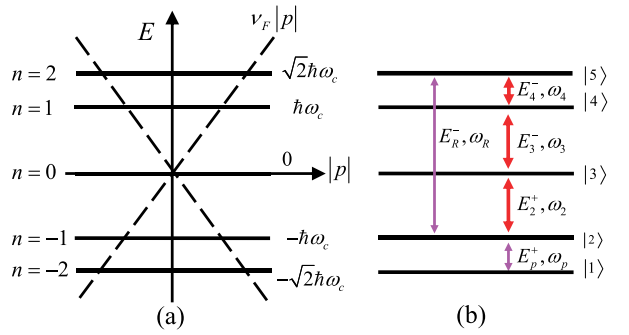

Fig. 1. (a) LLs near the Dirac point superimposed on the linear electron dispersion without the magnetic field $E = \pm v_F|p|$. The magnetic field condenses the original states in the Dirac cone into discrete energies. (b) Energy level diagram and optical transitions in graphene interacting with a weak probe pulse (with carrier frequency ω_p) and three cw pump fields (with carrier frequency $\omega_{2,3,4}$). The states $|1\rangle$, $|2\rangle$, $|3\rangle$, $|4\rangle$, and $|5\rangle$ correspond to the LLs with energy quantum numbers $n = -2, -1, 0, 1, 2$, respectively. The monolayer graphene is regarded as a perfect two-dimensional crystal structure in the x–y plane.

frequency ω_p (ω_2) constructs optical transitions $|1\rangle \leftrightarrow |2\rangle$ ($|2\rangle \leftrightarrow |3\rangle$), while the LHC-polarized component E_3^- (E_4^-) with carrier frequency ω_3 (ω_4) constructs optical transitions $|3\rangle \leftrightarrow |4\rangle$ ($|4\rangle \leftrightarrow |5\rangle$).

We begin our analysis by writing the wave function, i.e., $|\psi\rangle = A_1|1\rangle + A_2 e^{i(\vec{k}_p \cdot \vec{r})}|2\rangle + A_3 e^{i(\vec{k}_p + \vec{k}_2)\cdot\vec{r}}|3\rangle + A_4 e^{i(\vec{k}_p + \vec{k}_2 + \vec{k}_3)\cdot\vec{r}}|4\rangle + A_5 e^{i(\vec{k}_p + \vec{k}_R)\cdot\vec{r}}|5\rangle$, where A_j means the time-dependent probability amplitude in the corresponding subband $|j\rangle$. Under the rotating wave approximation and electric-dipole approximation, a set of equations of motion for these probability amplitudes can be written as

$$\dot{A}_2 = i(-\Delta_p + i\gamma_2)A_2 + i\Omega_p A_1 + i\Omega_2^* A_3 + i\Omega_R^* A_5, \quad (1)$$

$$\dot{A}_3 = i(-\Delta_3 + i\gamma_3)A_3 + i\Omega_2 A_2 + i\Omega_3^* A_4, \quad (2)$$

$$\dot{A}_4 = i(-\Delta_4 + i\gamma_4)A_4 + i\Omega_3 A_3 + i\Omega_4^* A_5 e^{-i\delta\vec{k}\cdot\vec{r}}, \quad (3)$$

$$\dot{A}_5 = i(-\Delta_5 + i\gamma_5)A_5 + i\Omega_R A_2 + i\Omega_4 A_4 e^{i\delta\vec{k}\cdot\vec{r}}, \quad (4)$$

where corresponding frequency detunings are defined as $\Delta_p = (\epsilon_{n=-1} - \epsilon_{n=-2})/\hbar - \omega_p$, $\Delta_3 = (\epsilon_{n=0} - \epsilon_{n=-2})/\hbar - (\omega_p + \omega_2)$, $\Delta_4 = (\epsilon_{n=1} - \epsilon_{n=-2})/\hbar - (\omega_p + \omega_2 + \omega_3)$, and $\Delta_5 = (\epsilon_{n=2} - \epsilon_{n=-2})/\hbar - (\omega_p + \omega_2 + \omega_3 + \omega_4)$. Corresponding Rabi frequencies for the relevant laser-driven intersubband transitions are represented as $\Omega_p = (\vec{\mu}_{21} \cdot \vec{e}_+)E_p^+/\hbar$, $\Omega_2 = (\vec{\mu}_{32} \cdot \vec{e}_+)E_2^+/\hbar$, $\Omega_3 = (\vec{\mu}_{43} \cdot \vec{e}_-)E_3^-/\hbar$, $\Omega_4 = (\vec{\mu}_{54} \cdot \vec{e}_-)E_4^-/\hbar$, and $\Omega_R = (\vec{\mu}_{52} \cdot \vec{e}_-)E_R^-/\hbar$, in which $\vec{\mu}_{mn} = \langle m|\vec{\mu}|n\rangle = e \cdot \langle m|\vec{r}|n\rangle = \frac{i\hbar e}{\epsilon_n - \epsilon_m}\langle m|v_F\vec{\sigma}|n\rangle$ denotes the dipole moments for transition between states $|m\rangle \leftrightarrow |n\rangle$. Moreover, $\delta\vec{k} = \vec{k}_2 + \vec{k}_3 + \vec{k}_4 - \vec{k}_R$ denotes a phase mismatching factor and $\gamma_i (i = 2, 3, 4, 5)$ corresponds to the decay rate of states $|i\rangle$.

In an appropriate frame, the initial population is assumed to occupy in the ground state $|1\rangle$ (i.e., the LL $n = -2$), which can be achieved by a doping hole [27,28]. When cw pump fields satisfy the resonant condition (i.e., $\Delta_3 = \Delta_4 = \Delta_5 = \Delta_p$), we can straightforwardly have the steady-state solutions of Eqs. (1)–(4) and slowly varying parts of polarization for weak probe and generated Raman fields:

$$P_p = N\mu_{21}A_2A_1^*/\epsilon_0 = \chi_p E_p, \quad (5)$$

$$P_R = N\mu_{52}A_5A_2^*/\epsilon_0 = P_R^{\mathrm{NL}} + P_{\mathrm{SRC}}^{\mathrm{NL}}E_R. \quad (6)$$

Here the symbol 'N' is defined as the 2D electron density of graphene and is also expressed as $N = n_s n_\nu N_\phi = 2/(\pi l_c^2)$ with the magnetic length l_c, in which the $n_s = -2$ and $n_\nu = -2$ are spin and valley degeneracy [29]. The polarization of generated Raman field and stimulated Raman scattering (SRC) are $P_R^{\mathrm{NL}} = \chi_R^{\mathrm{NL}}E_p^2E_2E_3E_4$ and $P_{\mathrm{SRC}}^{\mathrm{NL}} = \chi_{\mathrm{SRC}}^{\mathrm{NL}}E_p^2$, in which $\chi_p = N\mu_{21}^2(\Gamma_5^*\Omega_3^2 + \Gamma_3^*\Omega_4^2 - \Gamma_3^*\Gamma_4^*\Gamma_5^*)/(\epsilon_0\hbar S)$, $\chi_R^{\mathrm{NL}} = N\mu_{52}\mu_{21}^2\mu_{32}\mu_{43}\mu_{54}(\Gamma_5^*\Omega_3^2 + \Gamma_3^*\Omega_4^2 - \Gamma_3^*\Gamma_4^*\Gamma_5^*)/(\epsilon_0\hbar^5S^2)$ and $\chi_{\mathrm{SRC}}^{\mathrm{NL}} = N\mu_{52}^2\mu_{21}^2(\Gamma_3\Gamma_4 - \Omega_3^2)(\Gamma_5^*\Omega_3^2 + \Gamma_3^*\Omega_4^2 + \Gamma_3^*\Gamma_4^*\Gamma_5^*)/(\epsilon_0\hbar^3S^2)$ with $\Gamma_2 = -\Delta_p + i\gamma_2$, $\Gamma_j = -\Delta_j + i\gamma_j (j = 3, 4, 5)$ and $S = (\Gamma_3\Gamma_4 - \Omega_3^2)(\Gamma_2\Gamma_5 - \Omega_R^2) + (\Gamma_4\Gamma_5 - \Omega_4^2)(\Gamma_2\Gamma_3 - \Omega_2^2) - \Gamma_2\Gamma_3\Gamma_4\Gamma_5 - 2\mathrm{Re}(\Omega_2\Omega_3\Omega_4\Omega_R^*)$. Besides, the nonlinear susceptibility χ_R^{NL} (the so-called Raman gain factor) directly contributes to the Raman field generation, whereas the $\chi_{\mathrm{SRC}}^{\mathrm{NL}}$ is used to represent nonlinear susceptibility of SRC. For a 2D graphene, it makes sense to introduce the surface polarization P_R determined as an average dipole moment per unit area instead of unit volume. In principle, the generated Raman field E_R is governed by Maxwell's equation:

$$\partial_z E_R = i\omega_R P_R/(2c). \quad (7)$$

Because the polarization P_R is linear with the Raman field E_R, a general solution for Eq. (7) can be written as $E_R = E_0(e^{i\omega_R P_{\mathrm{RSC}}^{\mathrm{NL}} z/(2c)} - e^{-i\delta k\cdot z})$. In the limit of boundary condition $E_R|_{z=0} = 0$ and phase matching condition $\delta k = 0$, the generated Raman field can be obtained as

$$E_R = \frac{P_R^{\mathrm{NL}}(e^{i\omega_R N_{3D} P_{\mathrm{RSC}}^{\mathrm{NL}} z/(2Nc)} - 1)}{P_{\mathrm{SRC}}^{\mathrm{NL}}}, \quad (8)$$

where $N_{3D} = 2/(\Delta z \pi l_c^2) = N/\Delta z$ is the 3D density of electrons in graphene with the thickness Δz. When $\Delta z \sim z$, the above equation is effective for the 2D graphene system. In order to give a visualization for the intensity of the generated Raman field, we define the conversion efficiency of the generated Raman field as $\rho = (\Omega_R/\Omega_p)^2$.

Graphene, which is well-known for its linear and nonlinear effects, including optical saturable absorption and nonlinear refractive index [30,31], has been explored extensively in recent literature [19,20,29]. Specially for the magnetic field up to 3T, transition frequency ω_c dependent on magnetic field intensity is on the order of $\omega_c \simeq 10^{14}$ s^{-1}. In this scenario, $\omega_{52} \simeq 2.41 \times 10^{14}$ s^{-1} is located within the IR region. According to the numerical estimate in Refs. [19,26], decay rates can be estimated to be $\gamma_2 = \gamma_3 = \gamma_4 = \gamma_5 = 3 \times 10^{13}$ s^{-1}. Based on the realistic graphene parameters used in experiments [19,20], one general numerical estimation for the dipole moment between optical transition $|5\rangle \leftrightarrow |2\rangle$ ($|1\rangle \leftrightarrow |2\rangle$) is $|\vec{\mu}_{52}| \sim \hbar e v_F/(\epsilon_{n=2} - \epsilon_{n=-1}) \propto 1/\sqrt{B}$ ($|\vec{\mu}_{21}| \sim \hbar e v_F/(\epsilon_{n=-1} - \epsilon_{n=-2}) \propto 1/\sqrt{B}$). The electron concentration can be estimated to be $N \simeq 5 \times 10^{12}$ cm^{-2} and the substrate dielectric constant turns out to be $\epsilon_r \simeq 4.5$ [32].

Within the above practical parameter set, we first plot the linear susceptibility of probe field versus probe detuning for

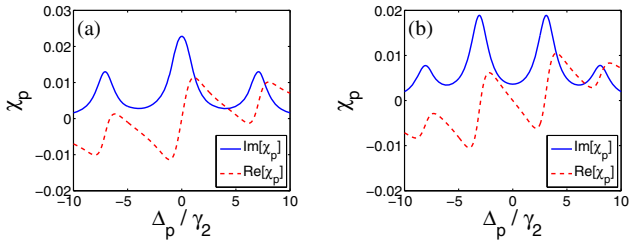

Fig. 2. Susceptibility of probe field versus probe detuning for different cw amplitude Ω_4; (a) $\Omega_4 = 0.5\gamma_2$; (b) $\Omega_4 = 5\gamma_2$. Other parameters are $\Omega_2 = \Omega_3 = 5\gamma_2$, $\Delta_3 = \Delta_4 = \Delta_5 = \Delta_p$, $\gamma_2 = \gamma_3 = \gamma_4 = \gamma_5 = 3 \times 10^{13}\ s^{-1}$, and $\Omega_p = 0.01\gamma_2$.

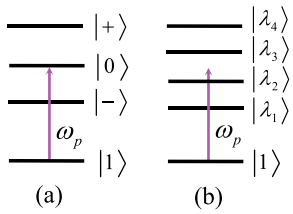

Fig. 3. Schematic of the dressed states. (a) Dressed states produced by states $|2\rangle$, $|3\rangle$, and $|4\rangle$ coupled with state $|1\rangle$ when the amplitude Ω_4 of the cw pump field is weak. (b) Dressed states produced by states $|2\rangle$, $|3\rangle$, $|4\rangle$, and $|5\rangle$ coupled with state $|1\rangle$ in the presence of a strong amplitude Ω_4 of a cw pump field.

different cw amplitude Ω_4, as shown in Fig. 2. When the cw pump field amplitude Ω_4 is weak [see Fig. 2(a)], one can find that this hyper-Raman process experiences a superluminal characteristic (i.e., anomalous dispersion) with a high absorption peak around the resonant probe frequency. If Ω_4 becomes a strong coherent control field [see Fig. 2(b)], an obvious transparency window with a subluminal characteristic (i.e., normal dispersion) is observed. The above interesting results come from the multiphoton quantum destructive interference caused by multiple excitation pathways between excited subbands and the ground state. This interference modifies the neighboring transitions and thus affects the absorption–dispersion property of the medium [2,3]. When the cw pump fields reach threshold value, a feedback excitation pathway $|1\rangle \rightarrow |2\rangle$ mediated by $|5\rangle$ is π out of phase with respect to a competing excitation pathway $|1\rangle \rightarrow |2\rangle$ [25]. Such a process simultaneously leads to the suppression for probe absorption.

Furthermore, these optical responses of linear susceptibility in a hyper-Raman process can be explained by dressed- states theory. To achieve a better Raman resonance, the cw pump fields are tuned exactly to the resonance frequencies and satisfy weak probe approximation $\Omega_{2,3,4} \gg \Omega_p$. First of all, for the case of Fig. 2(a) with $\Omega_{2,3} > \Omega_4$, one can safely neglect Ω_4 and the five-state system is decoupled to a four-level ladder-type configuration. Taking $|2\rangle$, $|3\rangle$, and $|4\rangle$ as three excited states, when they are coupled by two resonant cw pump fields $E_{2,3}$ to the ground state $|1\rangle$, these states split into three equivalent dress states [see Fig. 3(a)] as follows:

$$|0\rangle = \frac{\Omega_2}{\sqrt{\Omega_2^2 + \Omega_3^2}}|4\rangle - \frac{\Omega_3}{\sqrt{\Omega_2^2 + \Omega_3^2}}|2\rangle,$$
$$|\pm\rangle = \frac{1}{\sqrt{2}}\left(\pm|3\rangle + \frac{\Omega_3}{\sqrt{\Omega_2^2 + \Omega_3^2}}|4\rangle + \frac{\Omega_2}{\sqrt{\Omega_2^2 + \Omega_3^2}}|2\rangle\right), \quad \textbf{(9)}$$

where three energy eigenvalues are $\lambda_\pm = \pm\sqrt{\Omega_2^2 + \Omega_3^2}$ and $\lambda_0 = 0$. When the eigenfrequency $\omega_0 = (\epsilon_{n=0} - \epsilon_{n=-2})/\hbar$ couples to the ground state $|1\rangle$, a new dipole-allowed transition $|1\rangle \rightarrow |0\rangle$ induced by the cw pump fields creates the third absorption peak. For the second case of Fig. 2(b), as all of the cw pump fields are of sufficient intensity, its dress states can be immediately obtained as

$$|\lambda_i\rangle = \pm\frac{\Omega_3\Omega_4\lambda_i}{D}|5\rangle + \frac{\Omega_3\lambda_i^2}{D}|4\rangle \pm \frac{(\lambda_i^2 - \Omega_4^2)\lambda_i}{D}|3\rangle + \frac{\Omega_2(\lambda_i^2 - \Omega_4^2)}{D}|2\rangle \qquad (i = 1, 2, 3, 4), \quad \textbf{(10)}$$

with the term $D = \Omega_3^2\lambda_i^2(\Omega_4^2 + \lambda_i^2) + (\Omega_2^2 + \lambda_i^2)(\Omega_4^2 - \lambda_i^2)^2$ and the four energy eigenvalues of dressed states $\lambda_i = \pm\frac{1}{\sqrt{2}}\sqrt{\Omega_2^2 + \Omega_3^2 + \Omega_4^2 \pm \sqrt{(\Omega_2^2 + \Omega_3^2 + \Omega_4^2)^2 - 4\Omega_2^2\Omega_4^2}}$. Due to the superposition of multiple excitation pathways between a given set of optically coupled states, three transparency windows [see Fig. 3(b)] are expected to be established as a result of multiphoton destructive interference. This kind of linear optical response can be seen as an EIT-related phenomenon.

Now we pay our attention to the polarization that associates with the generation of the Raman field. Therefore, we plot the polarization of the generated Raman field versus probe detuning, as shown in Fig. 4. For a quantitative comparison between Figs. 4(a) and Fig. 4(b), a steep real part of polarization and a larger negative imaginary polarization imply that polarization of the generated Raman field is well-developed in the non-EIT window [see Fig. 4(a)]. However, the polarization is suppressed with the existence of EIT, as shown in Fig. 4(b). Physically, this polarization, resulting from the interaction between all optical fields and graphene, contributes to the hyper-Raman process. When a strong EIT changes the overall system response, the probe pulse no longer participates in the interaction of the system, and then the nonlinear Raman process is cut off. As a matter of fact, this is a consequence of the competition between the EIT effect and the hyper-Raman scattering process.

To give a better insight on the above mentioned competition behavior between two nonlinearity processes, in Fig. 5, we plot the efficiency of the generated Raman field as a function of three amplitudes of cw pump fields. According to the analysis of dressed states, when the amplitude of cw pump field Ω_4 is within low-light intensity (i.e., $\Omega_4 < 1.5\gamma_2 \simeq 29$ meV), one can find that a high efficiency of the generated Raman field coincides with a high probe absorption peak at resonant

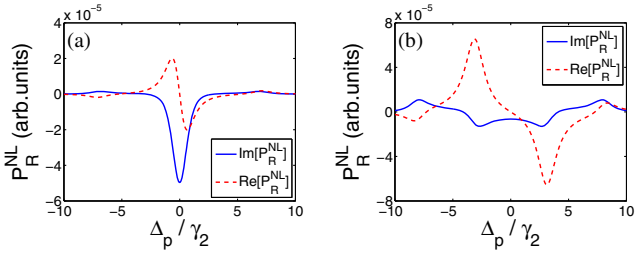

Fig. 4. Polarization of generated Raman field versus probe detuning. (a) $\Omega_4 = 0.5\gamma_2$; (b) $\Omega_4 = 5\gamma_2$. Other parameters are the same as in Fig. 2.

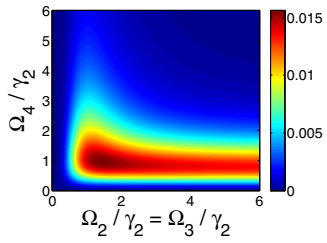

Fig. 5. Contour maps of the efficiency of generated Raman field as a function of the amplitudes of cw pump fields Ω_2, Ω_3, and Ω_4. Other parameters are the same as in Fig. 2.

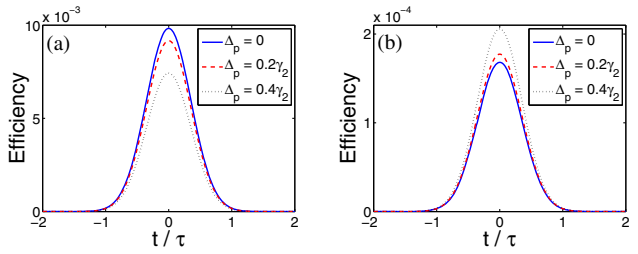

Fig. 6. (a) Efficiency of generated Raman field versus the normalized time t/τ for different probe detuning. (a) $\Omega_4 = 0.5\gamma_2$; (b) $\Omega_4 = 5\gamma_2$. Other parameters are the same as in Fig. 2.

frequency of the probe field [see Fig. 2(a)]. For this case, the probe pulse is depleted to support hyper-Raman scattering. However, as the amplitude of the cw pump field Ω_4 is sufficient enough (i.e., $\Omega_4 > 1.5\gamma_2$), the EIT will play an important role in the optical nonlinearity process, leading to a wide platform of low efficiency. In other words, the multiphoton destructive interference driven by a strong cw pump field destroys the channel for the hyper-Raman process and suppresses the efficiency of the generated Raman field.

Since the probe field and the generated Raman signal are in the form of optics pulses, it is necessary to simulate a practical approach. We assume that a Gaussian-shaped light beam i.e., $\Omega_p(t) = \Omega_p(0)e^{(-t^2/\tau^2)}$ with the pulse width τ is perpendicularly incident to the graphene structure under an external magnetic field. Before the simulation calculation, the efficiency needs to be rewritten as $\rho = |\Omega_R(t)/\Omega_p(0)|^2$ with the pulse width $\tau = 1$ ps fixed in graphene. We show the results from numerical simulations corresponding to a non-EIT and EIT parameter regions, as shown in Figs. 6(a) and 6(b). Again, it shows that the maximum efficiency of a generated Raman field can be achieved at low-light intensity [see Fig. 6(a)] by suppressing the EIT effect. In Fig. 6(b), it implies that the efficiency of generated Raman field increases when the system is far away from the center of the EIT window by increasing the probe detuning.

In conclusion, we have performed a competition between the EIT and hyper-Raman scattering based on the strong nonlinear optical response of graphene under a normal magnetic field. With the help of a dressed-state explanation, we reveal that the multiphoton destructive interference driven by a strong cw pump field plays a significant role in this competition between the EIT and the hyper-Raman process, in which an effective hyper-Raman scattering can be achieved via inhibiting EIT at a low-light intensity.

Funding. National Natural Science Foundation of China (NSFC) (11374050, 61372102); Scientific Research Foundation of Graduate School of Southeast University (YBJJ1522).

REFERENCES

1. Y. Wu and L. Deng, Phys. Rev. Lett. **93**, 143904 (2004).
2. W. X. Yang, J. M. Hou, and R. K. Lee, Phys. Rev. A **77**, 033838 (2008).
3. Y. Wu and X. Yang, Opt. Lett. **30**, 311 (2005).
4. H. Sun, S. Fan, H. Zhang, and S. Gong, Phys. Rev. B **87**, 235310 (2013).
5. W. X. Yang, Opt. Lett. **40**, 4903 (2015).
6. S. Kim, J. Jin, Y.-J. Kim, I.-Y. Park, Y. Kim, and S.-W. Kim, Nature **453**, 757 (2008).
7. Y. Wu, L. Wen, and Y. Zhu, Opt. Lett. **28**, 631 (2003).
8. M. Troccoli, A. Belyanin, F. Capasso, E. Cubukcu, D. L. Sivco, and A. Y. Cho, Nature **433**, 845 (2005).
9. S. E. Harris and L. V. Hau, Phys. Rev. Lett. **82**, 4611 (1999).
10. M. Fleischhauer, A. Imamoglu, and J. P. Marangos, Rev. Mod. Phys. **77**, 633 (2005).
11. M. Phillips and H. Wang, Phys. Rev. Lett. **89**, 186401 (2002).
12. M. Phillips, H. Wang, I. Rumyantsev, N. H. Kwong, R. Takayama, and R. Binder, Phys. Rev. Lett. **91**, 183602 (2003).
13. M. O. Scully, Nature **426**, 610 (2003).
14. K. I. Harada, T. Kanbashi, M. Mitsunaga, and K. Motomura, Phys. Rev. A **73**, 013807 (2006).
15. G. S. Agarwal and T. N. Dey, Phys. Rev. A **74**, 043805 (2006).
16. H. Nagai and T. Nakanaga, Phys. Rev. A **84**, 063408 (2011).
17. N. V. Hung, M. Trippenbach, E. Infeld, and B. Malomed, Phys. Rev. A **90**, 023841 (2014).
18. D. S. L. Abergel and V. I. Fal'ko, Phys. Rev. B **75**, 155430 (2007).
19. X. H. Yao and A. Belyanin, Phys. Rev. Lett. **108**, 255503 (2012).
20. M. Tokman, X. H. Yao, and A. Belyanin, Phys. Rev. Lett. **110**, 077404 (2013).
21. R. R. Nair, P. Blake, A. N. Grigorenko, K. S. Novoselov, T. J. Booth, T. Stauber, N. M. R. Peres, and A. K. Geim, Science **320**, 1308 (2008).
22. A. H. Castro Neto, F. Guinea, N. M. R. Peres, K. S. Novoselov, and A. K. Geim, Rev. Mod. Phys. **81**, 109 (2009).
23. M. Yankowitz, J. Xue, D. Cormode, J. D. Sanchez-Yamagishi, K. Watanabe, T. Taniguchi, P. Jarillo-Herrero, P. Jacquod, and B. J. LeRoy, Nat. Phys. **8**, 382 (2012).
24. M. L. Sadowski, G. Martinez, M. Potemski, C. Berger, and W. A. de Heer, Phys. Rev. Lett. **97**, 266405 (2006).
25. L. Deng, M. G. Payne, and W. R. Garrett, Phys. Rep. **429**, 123 (2006).
26. Z. Jiang, E. A. Henriksen, L. C. Tung, Y. J. Wang, M. E. Schwartz, M. Y. Han, P. Kim, and H. L. Stormer, Phys. Rev. Lett. **98**, 197403 (2007).
27. I. Gierz, C. Riedl, U. Starke, C. R. Ast, and K. Kern, Nano Lett. **8**, 4603 (2008).
28. G. Giovannetti, P. A. Khomyakov, G. Brocks, V. M. Karpan, J. van den Brink, and P. J. Kelly, Phys. Rev. Lett. **101**, 026803 (2008).
29. X. Yao and A. Belyanin, J. Phys. **25**, 054203 (2013).
30. Y. F. Song, H. Zhang, L. M. Zhao, D. Y. Shen, and D. Y. Tang, Opt. Express **20**, 23201 (2012).
31. H. Zhang, S. Virally, Q. Bao, L. K. Ping, S. Massar, N. Godbout, and P. Kockaert, Opt. Lett. **37**, 1856 (2012).
32. M. L. Nesterov, J. Bravo-Abad, A. Y. Nikitin, F. J. Garcia-Vidal, and L. Martin-Moreno, Laser Photon. Rev. **7**, L7 (2013).